

# Impedance measurement of single-crystalline and polycrystalline manganese–zinc ferrites with various non-stoichiometries

H. INABA

Technical Research Laboratories, Kawasaki Steel Corporation, 1 Kawasaki-Chou, Chuo-Ku, Chiba, 260, Japan

The impedance of both single-crystalline and polycrystalline manganese–zinc ferrite samples has been measured as a function of oxygen non-stoichiometry and the impedance of the bulk and the grain boundary has been analysed as a function of oxygen non-stoichiometry. The impedance of the single crystal increased in order along (1 0 0), (1 1 0) and (1 1 1) planes. Both the bulk and the grain boundary resistance increased with the oxygen non-stoichiometry, and the impedance for a higher impedance sample decreased at lower frequency due to the contribution of the capacitive component of the grain-boundary. The grain-boundary resistance increased more sharply with the non-stoichiometry than the bulk resistance due to the higher sensitivity to oxidation in the grain boundary. The grain boundary capacitance was about three orders of magnitude larger than the bulk capacitance and the both were almost constant against the non-stoichiometry.

## 1. Introduction

Manganese–zinc ferrites have been widely used in electronic applications such as transformers, choke coils, noise filters and recording heads, because of their high magnetic permeabilities and low magnetic losses. The importance of the control of oxygen partial pressure in the sintering process of Mn–Zn ferrites has been recognized in order to obtain materials of good magnetic qualities [1, 2], because the equilibrium oxygen partial pressure of Mn–Zn ferrites varies greatly in the temperature range of sintering [3–7]. It is very important to study the magnetic properties as a function of oxygen non-stoichiometry, because oxygen non-stoichiometry is not only related to the oxygen partial pressure during sintering but also to the  $\text{Fe}^{2+}$  content in the bulk and the grain boundary, which would greatly affect the magnetic properties. However, only a few studies on the relation between oxygen non-stoichiometry and magnetic properties have been performed [5–8].

The effect of oxygen non-stoichiometry on physical and magnetic properties of an Mn–Zn ferrite, using annealed samples under various oxygen pressures and temperatures has been studied by the present author [5], and it was found that Mn–Zn ferrites have two different defect structures: cation vacancies in a cation-deficient region and oxygen vacancies in an anion-deficient region, and the magnetic properties are optimum around the stoichiometric composition.

Otsuki and co-workers [9, 10] studied the relation between the power loss and the a.c. resistivity of Mn–Zn ferrites, analysing the power loss and the impedance as a function of frequency, but no separate

values of the resistive and capacitive part on the bulk and the grain boundary were reported. Yoo *et al.* [11] reported the bulk and the grain boundary impedance separately for Mn–Zn ferrites with various manganese contents. However, these studies were conducted by using polycrystalline samples only, and without changing oxygen non-stoichiometry.

In this study, the impedance of both single-crystalline and polycrystalline Mn–Zn ferrite samples was measured as a function of oxygen non-stoichiometry and the impedance of the bulk and the grain boundary has been analysed as a function of oxygen non-stoichiometry.

## 2. Experimental procedure

Polycrystalline Mn–Zn ferrite in the formula  $\text{Zn}_{0.26}\text{n}_{0.68}\text{Fe}_{2.06}\text{O}_4$  was prepared by the usual ceramic techniques. The mixture of  $\alpha\text{-Fe}_2\text{O}_3$ ,  $\text{Mn}_3\text{O}_4$  and ZnO in an appropriate metal composition was ground to mix in a ball mill, pre-fired for 1 h at 1173 K using a box-type furnace, ground to 1.2  $\mu\text{m}$  in a ballmill with the addition of 550 p.p.m.  $\text{CaCO}_3$  and 100 p.p.m.  $\text{SiO}_2$ , and pressed into the shape of a rectangular prism. The pressed samples were sintered for 3 h at 1593 K under an oxygen partial pressure of 0.05 bar and cooled at 200  $\text{K h}^{-1}$  under the same oxygen partial pressure until 1373 K, and under a nitrogen gas flow until room temperature, using a box-type furnace. The oxygen partial pressure was controlled by flowing a mixture of oxygen and nitrogen gases with a fixed ratio using mass-flow controllers. The size of the sintered rectangular prism was typically

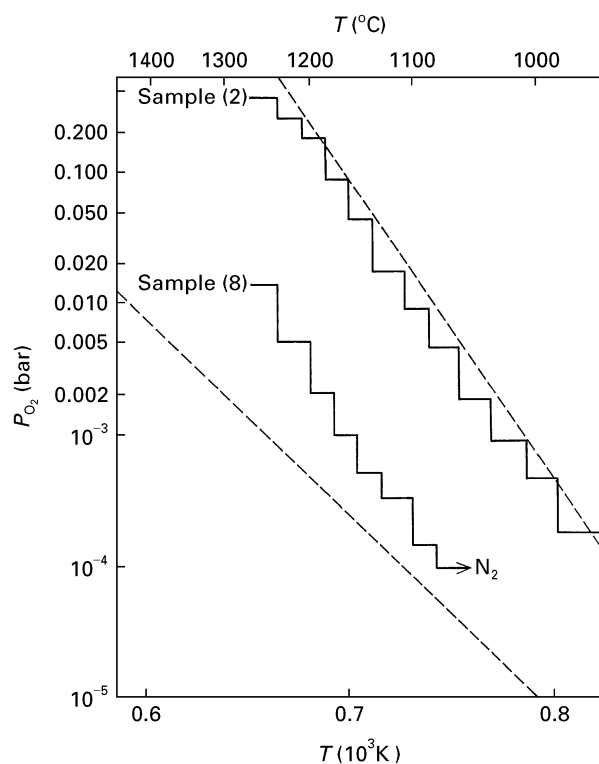


Figure 1 The Annealing programme for various non-stoichiometric samples. The heating part is not shown in the figure. After being kept for 8 h at 1523 K, the sample was kept at the programmed temperature and oxygen pressure shown in the figure. Below 950 K, the atmosphere was changed to a flow of nitrogen gas and the cooling rate was  $200 \text{ K h}^{-1}$ . (---) Phase boundaries according to Morineau and Paulus [3,4].

5 mm × 15 mm × 25 mm and was cut and polished to 9 mm × 9 mm × 0.5 mm for the impedance measurement. A single-crystalline sample of Mn–Zn ferrite in the formula  $\text{Zn}_{0.26}\text{Mn}_{0.68}\text{Fe}_{2.06}\text{O}_4$  was provided from Nihon Kesshou Kougaku Corporation and it was cut to 3 mm × 4 mm × 5 mm along the (100), (110) and (111) plane, which was then cut and polished to 1 mm × 4 mm × 5 mm for the impedance measurement. The both single-crystalline and polycrystalline samples were heated in the same furnace at  $200 \text{ K h}^{-1}$  upto 1523 K under an oxygen partial pressure of 0.05 bar and then annealed at various oxygen pressures and temperatures as shown in Fig. 1. Sample 8, for example, was kept for 8 h at 1523 K under 0.015 bar  $P_{\text{O}_2}$ , at 1498 K under 0.005 bar of  $P_{\text{O}_2}$  and successively at lower oxygen pressures and temperatures according to the programme shown in Fig. 1, which follows nearly a constant amount of  $\text{Fe}^{2+}$  line according to Morineau and Paulus [3, 4]; or equivalently, an iso-compositional line. Because the control of oxygen pressure below  $10^{-4}$  bar was difficult, nitrogen gas was flowed below 1323 K at the cooling rate of  $200 \text{ K h}^{-1}$ . For the whole annealing process it took about 24 h. The non-stoichiometry of the annealed samples was determined by the weight change during annealing. The estimated error in the determination of the non-stoichiometry,  $\delta$ , in  $(\text{Fe, Mn, Zn})_3\text{O}_{4+\delta}$  was about 0.0012. The density of samples ranged from  $4.93\text{--}4.94 \text{ g cm}^{-3}$ , while that before annealing was  $4.88 \text{ g cm}^{-3}$ . The X-ray diffraction pattern of these

samples showed a cubic spinel phase and the lattice constant of the polycrystalline samples was determined as 0.849 67, 0.849 76, 0.849 82, 0.849 76, and 0.849 57 nm, for samples p-2, p-5, p-8, p-10 and p-12, respectively. Samples p-2 and s-2 only, which were annealed at the highest oxygen partial pressures in this study, had small  $\alpha\text{-Fe}_2\text{O}_3$  peaks in addition to the spinel peaks. The ratio between  $\text{Fe}^{2+}$  and total iron was determined for these samples by chemical analysis [12, 13]. The estimated errors for the analysis of  $\text{Fe}^{2+}$  and total iron were 0.05% and 0.06%, respectively.

For the impedance measurement, copper lead wire was wound and attached to the both ends of the sample and silver paste was spread uniformly and then the sample was kept at 353 K for 1 h in air. The impedance was measured from 100 Hz to 40 MHz at room temperature by the two-probe method using an impedance analyser.

### 3. Results

The relative compositional change during annealing was obtained from the measurement of weight change before and after annealing. The relation between  $\text{Fe}^{2+}$  content and oxygen non-stoichiometry thus calculated is shown in Fig. 2. As discussed in the previous paper [5], oxygen non-stoichiometry was divided into the cation-deficient and oxygen-deficient regions and the stoichiometric composition was determined as the intersecting point of the two regions.

The results of the impedance measurement for the single-crystalline samples are shown in Fig. 3. The impedance increased as the non-stoichiometry,  $\delta$ , increased. The exceptionally high impedance of sample s-2, which has the highest  $\delta$  in the present study, is considered to be due to the presence of  $\alpha\text{-Fe}_2\text{O}_3$  in addition to the spinel phase. The magnitude of the impedance was varied within one order of magnitude except for the s-2 sample. For the nearly stoichiomet-

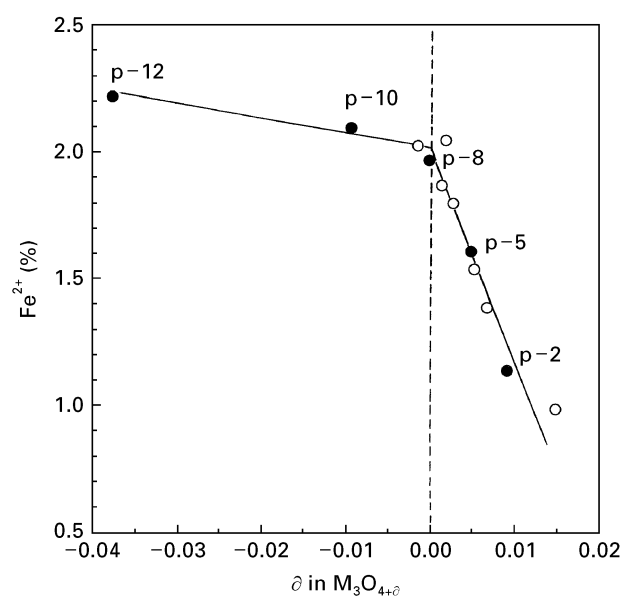


Figure 2 The relation between  $\text{Fe}^{2+}$  content and oxygen non-stoichiometry for the polycrystalline samples. (●) and the symbols p-n show the samples for the impedance measurement.

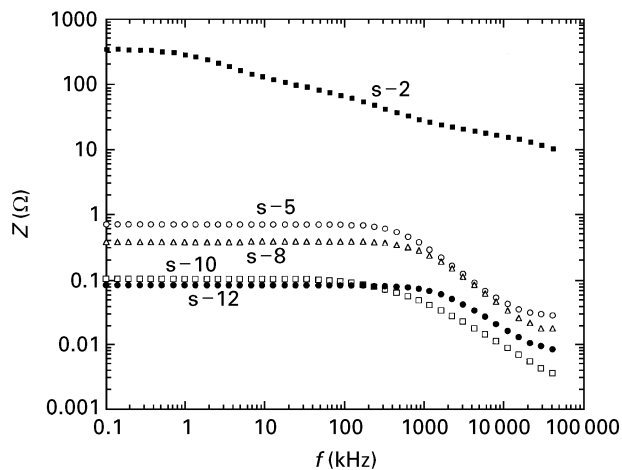


Figure 3 The impedance of single-crystalline samples with various non-stoichiometry as a function of frequency. The symbols  $s-n$  with the same  $n$  as  $p-n$  in Fig. 2 show the samples obtained from the same annealing conditions.

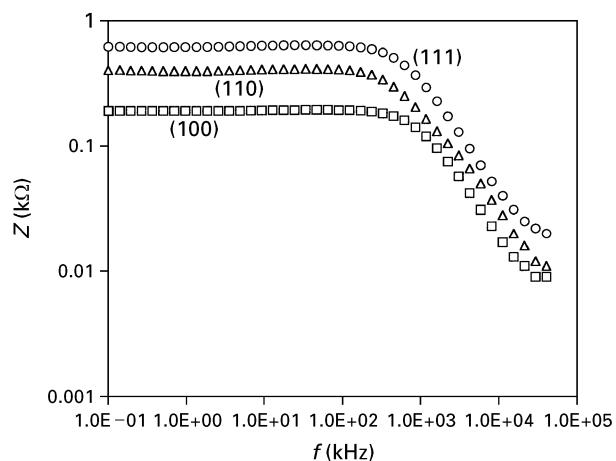


Figure 4 The impedance of single-crystalline samples, s-8, with nearly stoichiometric composition along the (100), (110) and (111) planes.

ric composition, s-8, the impedance measurement was conducted along three different planes, (100), (110) and (111), and the results are shown in Fig. 4. The magnitude of the impedance was in the order (111), (110) and (100). Namba *et al.* [14] studied the dependence of initial permeability of single-crystalline Mn–Zn ferrites on crystallographic orientation and found that the permeability was independent of the crystallographic orientation. From the point of view of electron hopping between  $\text{Fe}^{2+}$  and  $\text{Fe}^{3+}$  ions, in octahedral sites, the electrical conduction along the (110) plane would be most favourable, but the experimental results show that the highest conductive plane was (100). The reason for this is not known at present.

The results of the impedance measurement for the polycrystalline samples are shown in Fig. 5. The exceptionally high impedance of sample p-2 is also considered to be due to the presence of  $\alpha\text{-Fe}_2\text{O}_3$  in addition to the spinel phase. The impedance increased and the frequency at which the impedance begins to decrease, decreased as the non-stoichiometry,  $\delta$ , increased. The impedance at 0.1 kHz and the frequency

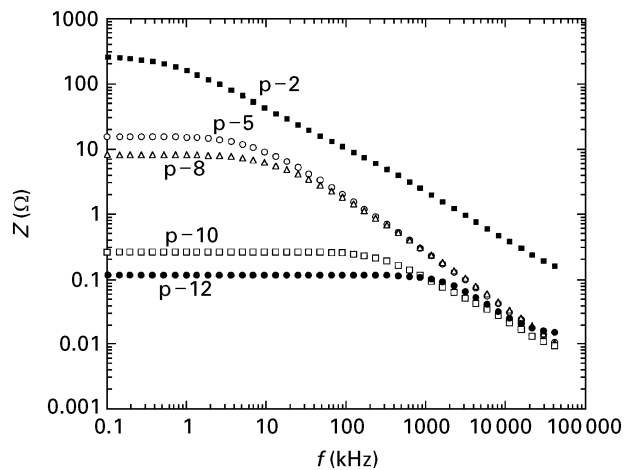


Figure 5 The impedance of polycrystalline samples with various non-stoichiometry as a function of frequency.

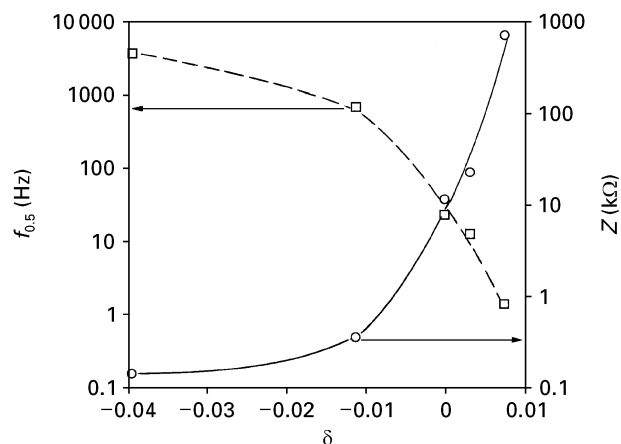


Figure 6 The impedance at 0.1 kHz and the frequency at which the impedance becomes half of that at 0.1 kHz as a function of oxygen non-stoichiometry for polycrystalline samples.

at which the impedance becomes half for the polycrystalline samples, are plotted as a function of non-stoichiometry in Fig. 6. The impedance of the higher impedance sample decreased at lower frequency due to the contribution of the capacitive component of the grain boundary. The variations of the magnitude of the impedance and the frequency at which the impedance begins to decrease for the polycrystalline samples were considerably larger than those in the case of the single crystal.

## 4. Discussion

### 4.1. Analysis of the impedance

The Cole–Cole plot of sample p-5, for example, is shown in Fig. 7, where a severely deformed semi-circle is seen. It was not possible to divide it into two semi-circles, one from the contribution due to the bulk and the other from that due to the grain boundary. This is considered to be due to fact that the difference in the magnitude of the impedance between the bulk and the grain boundary is not very much: about two orders of magnitude difference between s-5 and p-5 sample, for example, as seen from Figs 3 and 5.

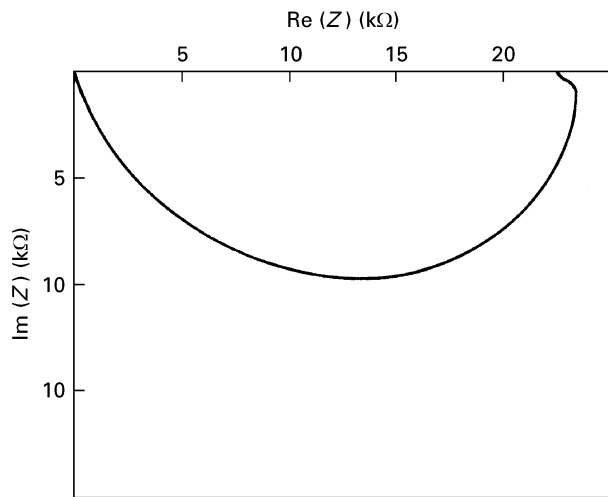


Figure 7 The Cole-Cole plot of the p-5 sample. The horizontal and vertical axes show the real part and imaginary part of the impedance, respectively.

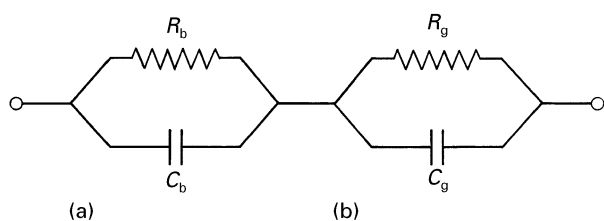


Figure 8 An equivalent circuit for polycrystalline Mn-Zn ferrites: (a) bulk, (b) grain boundary.

The analysis of the impedance was made by assuming the equivalent circuit shown in Fig. 8. The real and imaginary part of the impedance  $\text{Re}(Z)$  and  $\text{Im}(Z)$  are written as

$$\text{Re}(Z) = \frac{R_b}{1 + \omega^2 C_b^2 R_b^2} + \frac{R_g}{1 + \omega^2 C_g^2 R_g^2} \quad (1)$$

$$\text{Im}(Z) = \frac{-R_b^2 \omega C_b}{1 + \omega^2 C_b^2 R_b^2} + \frac{-R_g^2 \omega C_g}{1 + \omega^2 C_g^2 R_g^2} \quad (2)$$

The real and imaginary part of the impedance of polycrystalline samples were obtained from the observed impedance and the phase shift, and  $R_b$ ,  $R_g$ ,  $C_b$  and  $C_g$ , the resistance and capacitance of bulk and grain boundary, were obtained by fitting these values to the experimentally observed real and imaginary part of the impedance using Equations 1 and 2. The fitting of the real and imaginary part of the impedance of sample p-5, for example, are shown in Figs 9 and 10, respectively. From these the resistances for the bulk and the grain boundary,  $R_b$  and  $R_g$ , were determined as 22.4 kΩ and 300 Ω, respectively, and the capacitances for the bulk and the grain boundary,  $C_b$  and  $C_g$ , were determined as  $4.5 \times 10^{-10}$  and  $1.0 \times 10^{-6}$  F. For the determination of  $C_b$ , the impedance data of single crystals were used, because the fitting to the polycrystalline data was less sensitive to the variation of  $C_b$  and the error of the determination was large. The analysis using the equivalent circuit was not conducted for the sample p-2, because it contains  $\alpha\text{-Fe}_2\text{O}_3$  in addition to the spinel phase, and the impedance can-

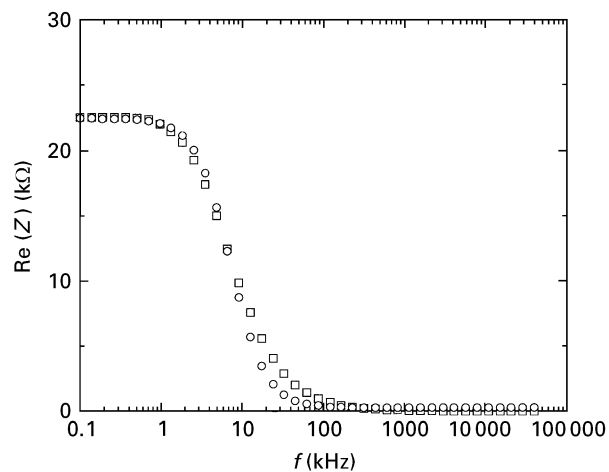


Figure 9 Fitting of the real part of the impedance for p-5 sample using Equations 1 and 2. (○) Measured data, (□) calculated data.

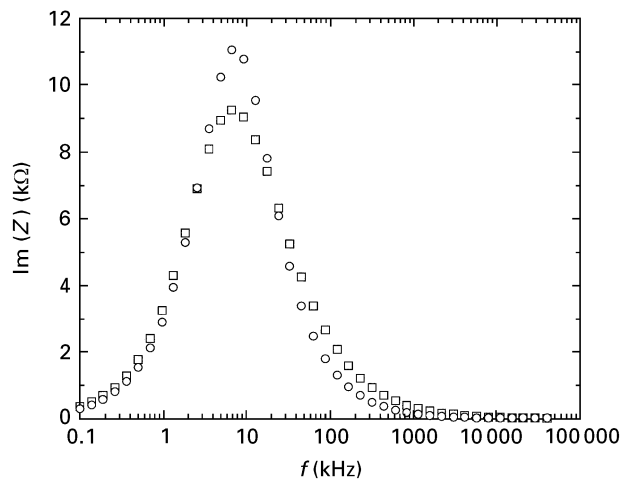


Figure 10 Fitting of the imaginary part of the impedance for p-5 sample. (○) Measured data, (□) calculated data.

not be described as the equivalent circuit shown in Fig. 8.

The resultant resistances for the bulk and the grain boundary,  $R_b$  and  $R_g$ , are shown in Fig. 11 as a function of non-stoichiometry,  $\delta$ . It is seen from Fig. 11 that both the bulk and the grain boundary resistances increase sharply around the stoichiometric composition, but the grain boundary resistance increases more sharply than the bulk resistance; about one order of magnitude larger comparing p-5 with p-12 in the case of  $R_b$ , and about two orders of magnitude larger comparing p-5 with p-12 in the case of  $R_g$ . This is considered to be due to the fact that the grain boundary is more easily oxidized when the oxygen partial pressure is higher during the annealing process. It is suggested from these results that during the last stage of sintering, in the cooling process the selective oxidation of the grain-boundary keeping the  $\text{Fe}^{2+}$  content of the bulk at an optimum level is desirable and possible. The resistivity of Mn-Zn ferrites is considered to be mainly determined by the hopping of electrons between  $\text{Fe}^{2+}$  and  $\text{Fe}^{3+}$  ions. This may also be true even in the grain boundary, because the composition analysis [15] of the grain-boundary showed

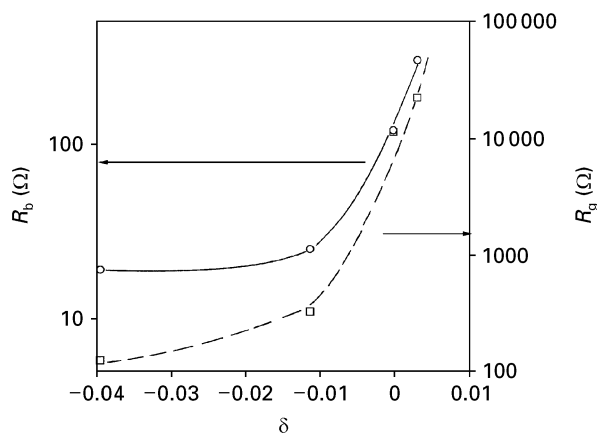


Figure 11 The bulk and the grain boundary resistance of polycrystalline samples,  $R_b$  and  $R_g$ , as a function of non-stoichiometry obtained from fitting as shown in Fig. 9.

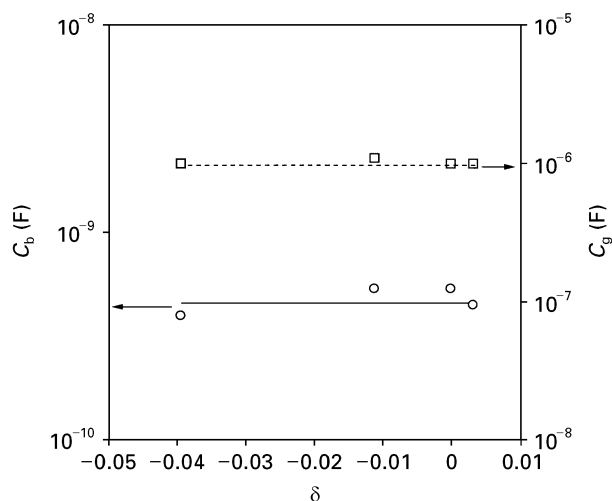


Figure 12 The bulk and the grain boundary capacitance of polycrystalline samples,  $C_b$  and  $C_g$ , as a function of non-stoichiometry obtained from fitting as shown in Fig. 10.

that the main component in the grain boundary was still iron, although the iron content was decreased, and additive atoms such as calcium and silicon were enriched around the grain boundary.

The capacitances for the bulk and the grain boundary,  $C_b$  and  $C_g$ , are shown in Fig. 12 as a function of non-stoichiometry,  $\delta$ . It is seen from Fig. 12 that both the bulk and the grain boundary capacitances are almost constant against non-stoichiometry,  $\delta$ . This result suggests that the capacitive component is independent of the oxygen non-stoichiometry for both the bulk and the grain boundary, and that the dielectric property is not sensitive to the small change in the composition.

#### 4.2. The relation between the optimum non-stoichiometry of Mn–Zn ferrites for magnetic properties and the property of the grain boundary

As described in the previous paper [5], permeability of Mn–Zn ferrites is maximum and power loss is minimum around the stoichiometric composition. Power

loss of Mn–Zn ferrites is considered to consist of the three terms hysteresis loss, eddy current loss and residual loss. Because permeability is maximum at the stoichiometric composition, hysteresis loss is thought to be minimum at the stoichiometric composition. In order to minimize the eddy current loss, it is desirable to maximize the electrical resistivity. However, both the bulk and the grain boundary resistance increase monotonically with the non-stoichiometry,  $\delta$ , as seen in Fig. 11, and the stoichiometric composition is not optimum in the view of the bulk and the grain boundary resistance. These results suggest that the bulk and the grain boundary impedance are not the predominant factor for magnetic properties, but other factors, such as the magneto-crystalline constant and the term due to internal stress, are important. The compositional dependence of the d.c. electrical resistivity was also measured by Morita and Okamoto [8], showing the maximum value at the stoichiometric composition [5]. The reason for the difference between their data and the present results is not clear, but may be due to the difference in sample preparation. At any rate, there is no large difference in electrical resistivity between the stoichiometric composition and those with positive  $\delta$ , as seen in Fig. 11. Therefore, the optimum composition for the sum of hysteresis loss and eddy current loss may be around the stoichiometric composition.

## 5. Conclusions

The impedance of both single-crystalline and polycrystalline Mn–Zn ferrite samples has been measured as a function of oxygen non-stoichiometry and the impedance of the bulk and the grain boundary have been analysed as a function of oxygen non-stoichiometry.

1. The impedance of the single-crystalline samples with nearly stoichiometric composition increased in the order along (1 0 0), (1 1 0) and (1 1 1) planes.

2. Both the bulk and the grain boundary resistance increased with the oxygen non-stoichiometry,  $\delta$ , in  $(\text{Fe, Mn, Zn})_3\text{O}_{4+\delta}$ , and the impedance of the higher impedance sample decreases at lower frequency due to the contribution of the capacitive component of the grain boundary.

3. The grain boundary resistance increased more sharply with the non-stoichiometry,  $\delta$ , than the bulk resistance due to the higher sensitivity to oxidation in the grain boundary. It is suggested that during the last stage of sintering, in the cooling process, the selective oxidation of the grain boundary keeping the  $\text{Fe}^{2+}$  content of the bulk to be an optimum level is desirable and possible.

4. The grain boundary capacitance was about three orders of magnitude larger than the bulk capacitance and both were almost constant against the non-stoichiometry,  $\delta$ .

5. The optimum non-stoichiometric composition for the optimum magnetic properties was slightly different from the composition to give the maximum impedance, suggesting the importance of other factors for the magnetic properties.

## References

1. H. INABA, in "Proceedings of 1993 Powder Metallurgy World Congress" edited by Y. Bando and K. Kosuge (Japan Society of Powder and Powder Metallurgy, Kyoto, 1993) p. 381.
2. I-N. LOIN, R. K. MUSHIER and G. THOMAS, *IEEE Trans. Mag.* **Mag-22** (1986) 175.
3. R. MORINEAU and M. PAULUS, *Phys. status solidi (a)* **20** (1973) 373.
4. *Idem*, *IEEE Trans. Mag.* **Mag-11** (1975) 1312.
5. H. INABA, *J. Am. Ceram. Soc.* **78** (1995) 2907.
6. T. TANAKA, *Jpn J. Appl. Phys.* **13** (1974) 1235.
7. *Idem*, *J. Am. Ceram. Soc.* **64** (1981) 419.
8. A. MORITA and A. OKAMOTO, in "Ferrites: Proceedings of The Third International Conference on Ferrites" edited by H. Watanabe, S. Iida and M. Sugimoto (Center for Academic Publication, Kyoto, 1980) p. 313.
9. E. OTSUKI, S. YAMADA, T. OTSUKA, K. SHOJI and T. SATO, *J. Appl. Phys.* **69** (1991) 5942.
10. S. YAMADA, E. OTSUKI and T. OTSUKA, *Tokin Tech. Rev.* **18** (1991) 16.
11. H. I. YOO, H. L. TULLER, J. A. WEIRICK and W. D. KEHR, in "Proceedings of the Symposium on Electro-Ceramics Solid-State Ionics" (1988) p. 71.
12. Japanese Industrial Standards, JIS M 8213-1983 (1983).
13. Japanese Industrial Standards, JIS M 8212-1983 (1983).
14. Y. NAMBA, N. IKAWA and M. GOHDA, *J. Jpn Soc. Precision Eng.* **54** (1988) 89.
15. H. INABA, T. ABE, Y. KITANO and J. SHIMOMURA, *J. Solid State Chem.* **121** (1996) 117.

*Received 7 September 1995  
and accepted 2 July 1996*